**Novel Ligand and Device Designs for Stable Light-Emitting Electrochemical Cells Based on Heteroleptic Copper(I) Complexes**

Elisa Fresta, Giorgio Volpi, Marco Milanesio, Claudio Garino, Claudia Barolo, Ruben D. Costá.

Novel Ligand and Device Designs for Stable Light-Emitting Electrochemical Cells Based on Heteroleptic Copper(I) Complexes

Inorganic Chemistry, 57, 2018, pagg. 10469-10479

DOI: 10.1021/acs.inorgchem.8b01914

# Novel Ligand and Device Designs for Stable Light-Emitting Electrochemical Cells Based on Heteroleptic Copper(I) Complexes

E. Fresta[a], G. Volpi[b], M. Milanesio[c,e], C. Garino[b], C. Barolo*[b,d], and R. D. Costá*[,a]

[a]IMDEA Materials Institute, Calle Eric Kandel 2, 28906 Getafe, Madrid, Spain
[b]Department of Chemistry, NIS Interdepartmental Centre and INSTM Reference Centre, Università degli Studi di Torino, Via Pietro Giuria 7, 10125 Torino, Italy
[c]Dipartimento di Scienze e Innovazione Tecnologica, Università del Piemonte Orientale, Viale T. Michel 11, I-15121 Alessandria, Italy
[d]ICxT Interdepartmental Centre, Università degli Studi di Torino, Lungo Dora Siena 100, 10153 Torino, Italy
[e]CrisDi, Interdepartmental Center for Crystallography, 10125 Turin, Italy

## Abstract

This work reports on the positive impact of (i) attaching methoxy groups at the ortho position of the bipyridine ligand (6,6′-dimethoxy-2,2′-bipyridine) in heteroleptic copper(I) complexes belonging to the [Cu(bpy)(POP)]+ family, and (ii) a new device design comprising a multilayered architecture to decouple hole/electron injection and transport processes on the performance of light-emitting electrochemical cells (LECs). In short, the substituted complex showed enhanced thermal- and photostability, photoluminescence, and ionic conductivity features in thin films compared to those of the archetypal complex without substitution. These beneficial features led to LECs outperforming reference devices in terms of luminance, stability, and efficacy. Furthermore, a new device design resulted in a 10-fold enhancement of the stability without negatively affecting the other figures of merit. Here, hole/electron injection and transport processes are performed at two different layers, while electron injection and electron−hole recombination occur at the copper(I) complex layer. As such, this work provides further insights into a smart design of N^N ligands for copper(I) complexes, opening the path to a simple device architecture toward an enhanced electroluminescence response.

## 1 Introduction

The final goal in thin-film lighting technologies is to fabricate highly efficient, air-stable, low-cost, and single-layer lighting sources using up-scalable solution-based techniques.[1−4]

Those requirements are fulfilled by the light-emitting electrochemical cell (LEC) technology.[1−3,5,6] LECs are a single-layer lighting device consisting of a mixture of a luminescent material and an ionic electrolyte. When no bias is applied, the mobile ions are randomly distributed in the active layer. Upon biasing the device, the ions drift toward the electrode interfaces, creating the so-called electric double layers (EDLs) that assist charge injection regardless of the nature of the electrodes, for example, air-stable metals, metal oxides, nanocarbon, etc.[2,3,7−9] As a result, highly conductive n- and p-doped regions along with a light-emitting nondoped region are formed.[10−12]

The most attractive LEC features are (i) tolerance with respect to the nature of the electrodes and the thickness of the active layer ranging from a few tens to hundreds of nanometers, (ii) easy fabrication from solution-based techniques under ambient conditions, for example, roll-to-roll,[13] inkjet printing,[14] spray-deposition,[15] etc., and (iii) versatility in emitters, such as polymers, ionic transition-metal complexes (iTMCs), small molecules, quantum dots, and perovskites.[2,3,6,16−20] In addition, the LEC community has also demonstrated the potential applicability of this lighting technology using unconventional conductive substrates, for example, kitchen forks,[15] printing papers,[21] wearable fibers,[22] line-art lighting devices,[23] etc. Finally, numerous research groups focused on the search of sustainable and low-cost emitters to fabricate highly efficient and stable LECs spanning the whole visible range,[1−3] including white-emitting LECs featuring promising performances.[16,24−26]

In this regard, copper(I)-based iTMCs (Cu-iTMCs) are attracting more and more attention, since they are considered as a serious alternative to the well-known iridium(III)-based iTMCs (Ir-iTMCs).[5,6] The interest in Cu-iTMCs is justified by (i) the absence of metal-centered (MC) excited states that are typical degradative pathways for iridium(III) complexes,[5,27−29] (ii) the emission mechanism involving a thermally activated delayed fluorescence (TADF) that results in high photoluminescence quantum yields (Φ),[30−32] (iii) the large number of emitting families,[3,33,34] and (iv) the low production costs related to the use of a relatively abundant and cheaper metal with respect to iridium.

Among the different Cu-iTMC families applied in LECs,[35−41] heteroleptic complexes−that is, $[Cu(N^N)(P^P)]^+$, where N^N and P^P are diimine and diphosphine ligands, respectively−are the most studied ones. Currently, huge efforts have been conducted to elucidate strategies with respect to both the synthesis protocol (purification and yields)[42,43] and the ligand design (para or ortho substitutions of the N^N ligand),[37−39,44] toward enhancing the performance of yellowand green-emitting LECs.

Concerning the ligand design, important achievements have been realized attaching σ-donating groups or halogen atoms at the para position of the N^N ligands.[39,44] For instance, a linear correlation between the σ-Hammett parameter ($\sigma_p$) and an improvement in the LEC figures of merit was recently reported.[44] As far as the substitution at the ortho position is concerned, Yersin's group has recently noted a significant enhancement of the photoluminescence upon attaching one or two methyl groups,[30] while Bolink and co-workers proved it in LECs.[37,38] This substitution causes the twisting of the bipyridyl units coupled with a tilting of the heterocyclic ring plane, leading to enhanced luminescence as the photoinduced flattening distortion is limited. Noteworthy, the stabilizing effect is more pronounced in symmetrically substituted complexes, while the substitution with groups that are bulkier than the ethyl moiety does not provide any further enhancement and renders the synthesis of pure complexes more difficult.[38]

Following these works, we propose a rationalized ligand design in which both ortho positions of the 2,2′-bipyridine ligand are functionalized with methoxy groups (6,6′-dimethoxy-2,2′-bipyridine, MeO-bpy). Two reasons compelled us to select this moiety. On one hand, ortho substitution with methoxy groups provides a stronger electron-donating effect than that of the methyl group. This should provide an enhanced backdonation that strengthens the metal−ligand coordination, preventing significant structural changes upon excitation. On the other hand, both the steric hindrance and easy rotation motion of the methoxy group further shields the coordination sphere of the Cu(I) metal ion. This should avoid the solventassisted ligand exchange process in coordinative solvents, increasing both thermal- and photostabilities.

The above statements were corroborated by comparing the spectroscopic and electrochemical features of two complexes, namely, the archetypal [Cu(bpy)(POP)][$PF_6$] (**1**) and the novel [Cu(MeO-bpy)(POP)][$PF_6$] (**2**), where bpy is 2,2′-bipyridine, MeO-bpy is 6,6′-dimethoxy-2,2′-bipyridine, and POP is bis(2-(diphenylphosphino)phenyl)ether (Figure 1). Here, efficiency and stability of LECs were enhanced up to three- to fourfold (**2** vs **1**). Furthermore, the device stability can be enhanced by 10-fold using a new device architecture to overcome the irreversible oxidation process of the CuiTMCs.[34,45−47] Overall, this work illustrates an easy way to improve the performance of LECs based on Cu-iTMCs through both novel ligand and device designs.

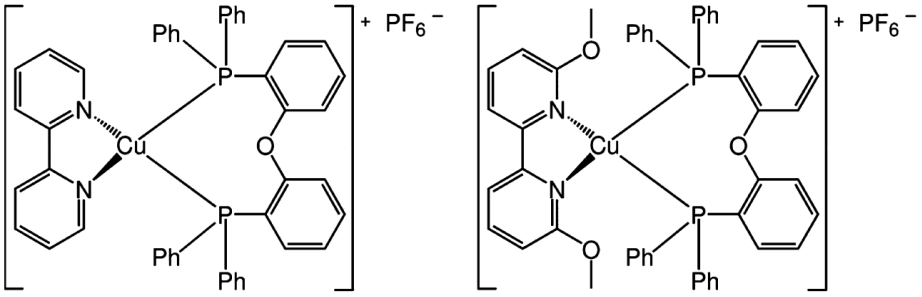


**Fig. 1.** Chemical structures of **1** (left) and **2** (right).

## 2 Results and discussion

### *2.1. Synthesis and X-ray Characterization.*

The synthesis of MeO-bpy was performed by one-pot microwave-assisted synthetic protocol with a yield of 80% and short time (90 min) compared to traditional synthetic pathways (74% and 18 h).[48] The formation of the final product was monitored through gas chromatography coupled with mass spectrometry (GC-MS) by stopping the reaction every 30 min, until a maximum in the mass spectrum of the reaction mixture was observed for the final product. The ligand was characterized by mass spectrometry and $^{1}H$ and $^{13}C$ NMR spectroscopy (Figures S1 and S2).

Interestingly, X-ray structure analysis of the ligand showed a planar anti conformation with a N1−C1−C1′−N1′ torsion angle of 180.4° (Figure S3 and Tables S1−S3). To explore the energetic cost of the rotation along NC2C2′N′ torsion angle, density functional theory (DFT) calculations were performed. The *trans* conformation resulted to be the more stable, as suggested by the crystal structure. The perfect *cis* conformation corresponds to an energy maximum with a relative energy of 8.0 kcal/mol (Figure S3 and Table S4). This maximum is energetically close to another relative energy minimum with N1−C1−C1′−N1′ torsion angle equal to 35° depicted in Figure S4 with a relative energy of 7.1 kcal/mol.

Complexes **1** and **2** were prepared in an excellent yield following procedures reported in literature.[40,49] $^{1}H$, $^{13}C$, and $^{31}P$ NMR spectroscopic and mass spectrometric characterizations confirmed the

formation of the desired heteroleptic complex **2** with no evidence of either the presence of homoleptic species or free ligands (Figure S5). The new complex 2 was crystallized from a solution of $H_2O$ and acetone 1:1 and its structure solved by X-ray diffraction (XRD), showing a P21/c space group (Figures 2 and S6−S8 and Tables 1 and S5−S7). The Cu(I) atom shows a nonplanar pseudo-tetrahedral coordination with the two P atoms of the POP moiety and the two N atoms of the bpy moiety (Figure 2), similarly to the parent compound **1**.[40] The Cu−P distances are 2.27 and 2.28 Å. The packing is arranged in planes of molecules of 2 alternated by $PF_6^-$ planes (Figure S8). Rather short CH···F contacts of ∼2.6 Å, that is, closer to the sum of the van der Waals radii of H and F, are observed. This arrangement might explain the preferred growth in two directions to form extended laminae, while in the third direction the growth is probably unfavored, since no regular rows of positive and negative ions are observed. The oxygen bridge between the two phenyls shows C−O distances of 1.39 Å, which are identical to those of an aromatic bond, suggesting a larger electronic delocalization across the bridge than that of 1.[45] This is reasonable taking into account the strong electron-donor role provided by the methoxy groups.

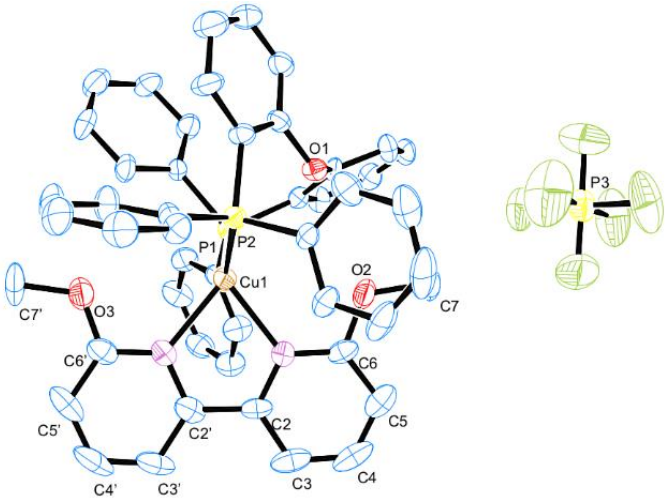


**Fig. 2.** X-ray structure of **2**.

As such, the ancillary ligand shows an almost planar conformation with a N1−C1−C1′−N1′ torsion angle of 6.22°. As reported elsewhere,[45] the X-ray structure of **1** shows similar Cu−P bond lengths of 2.25 and 2.24 Å, as well as similar Cu−N bond lengths of 2.07 and 2.05 Å. However, it differs from **2** in the overall distortion of the coordination sphere, assessed by measuring the P−Cu−X bond angles, where point X is defined (using crystallographic coordinates) as the midpoint of the C1−C1′ bond in each complex. Here, no distortion at all from the ideal tetrahedral geometry would result in an angle of 120°. The measured values are of 129.3° and 115.3° for **1**[45] and 125.6° and 118.2° for **2**. The latter are closer to the ideal angle, suggesting an enhanced molecular rigidity in the ground state.

**Table 1.** Crystal data and structure refinement of **2** and MeO-bpy.

| Compound | **2** | MeO-bpy |
|---|---|---|
| Empirical formula | $C_{48}H_{40}CuF_6N_2O_3P_3$ | $C_{12}H_{12}N_2O_2$ |
| Formula weight | 770.61 | 216.24 |
| Temperature | 293(2) K | |
| Wavelength | 0.71073 Å | |
| Crystal system | Monoclinic | Orthorhombic |
| Space group | P 21/n | P n 21 a |
| Unit cell dimensions (edges in Å and angles in °) | a = 9.8718(15)<br>b = 29.021(5)<br>c = 15.241(2)<br>β= 95.469(14) | a = 12.5060(14)<br>b = 21.731(3)<br>c = 3.9733(7) |
| Volume $Å^3$ | 4346.7(11) | 1079.8(3) |
| Z | 5 | 4 |
| Density ($Mg/m^3$ calculated) | 1.472 | 1.330 |
| Absorption coefficient ($mm^{-1}$) | 0.684 | 0.092 |
| F(000) | 1976 | 456 |
| Crystal size ($mm^3$) | 0.120 x 0.040 x 0.020 | 0.410 x 0.220 x 0.040 |
| Theta range for data collection | 2.807 to 28.605°. | 3.258 to 28.033°. |
| Reflections collected | 37346 | 6417 |
| Independent reflections | 10063 [R(int) = 0.2518] | 2396 [R(int) = 0.0636] |
| Completeness to theta = 25.242° | 99.8 % | 99.9 % |
| Refinement method | Full-matrix least-squares on $F^2$ | |
| Data / restraints / parameters | 10063 / 0 / 570 | 2396 / 1 / 123 |
| Goodness-of-fit on F2 | 0.955 | 1.037 |
| Final R indices [I>2sigma(I)] | R1 = 0.0876, wR2 = 0.1692 | R1 = 0.1122, wR2 = 0.2687 |
| R indices (all data) | R1 = 0.2908, wR2 = 0.2576 | R1 = 0.1875, wR2 = 0.3380 |
| Largest diff. peak and hole | 0.605 and –0.488 e.$Å^{-3}$ | 0.797 and –0.301 e.$Å^{-3}$ |

*2.2. Spectroscopic Characterization.*

As shown in Figures 3 and 4, fresh acetonitrile solutions of both **1** and **2** showed two well-defined absorption bands corresponding to ligand-centered (LC) and metal-to-ligand charge transfer (MLCT) transitions located at 280−300 and 380−400 nm regions, respectively. In general, the absorption maxima of **2** are red-shifted (15 nm) compared to those of **1**, highlighting the electron-donating features of the methoxy groups (Table 2). In particular, we noted a clear solvatochromic effect while comparing the absorption features of both complexes in dichloromethane and acetonitrile solutions (Figures 3, 4, and S9, as well as Table 2). Blue and red shifts for all the absorption maxima were observed for **1** and **2**, respectively. In addition, the MLCT band of **2** is clearly noted in dichloromethane rather than in acetonitrile. These account for a larger dipole moment in both the excited and ground states of **2** compared to those of 1.[46] Next, the thermal and photostabilities of both complexes in acetonitrile ($5 \cdot 10^{-4}$ M), due to its well-known coordinative character, were investigated. First, the absorption features were monitored over time at 70 °C in dark (Figure 3). Under these conditions, ligand exchange of the diimine ligand by solvent molecules is facilitated leading to the formation of undesired $[Cu(POP)(MeCN)_2]^+$ and homoleptic $[Cu(bpy)_2]^+$ species (MeCN refers to

acetonitrile).[46,50] This is attested by both a decrease of the MLCT band intensity and the appearance of a new band at ~330 nm that has been previously ascribed to the homoleptic diimine complexes.[33,51] This is only observed for **1** in a time frame of a few hours, while **2** does not show any significant change in this time frame (Figure 3). Thus, both the sterical hindrance and the free motion of the methoxy efficiently prevent the degradation of the complex.

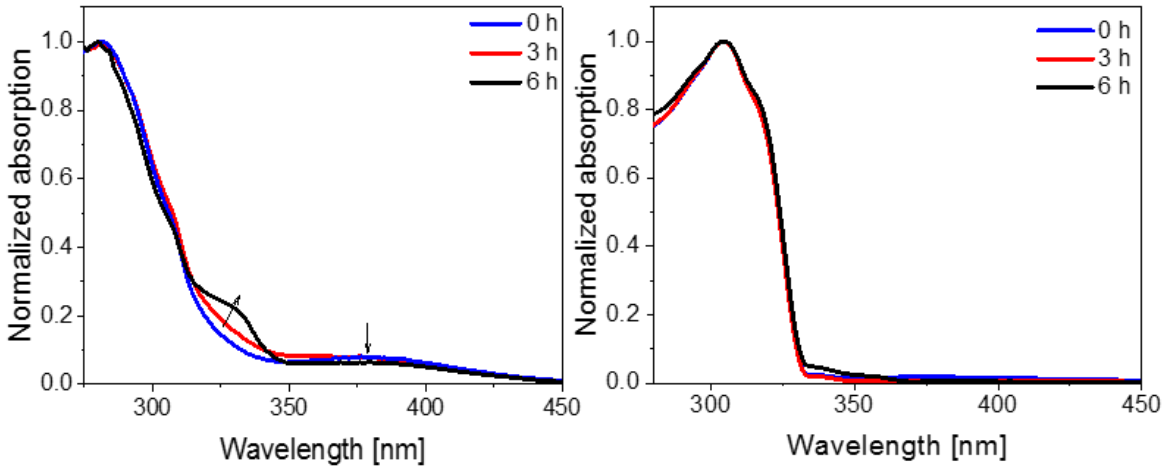


**Fig. 3.** Changes of the UV − vis absorption spectra of **1** (left) and **2** (right) measured in acetonitrile over time at 70 °C in dark.

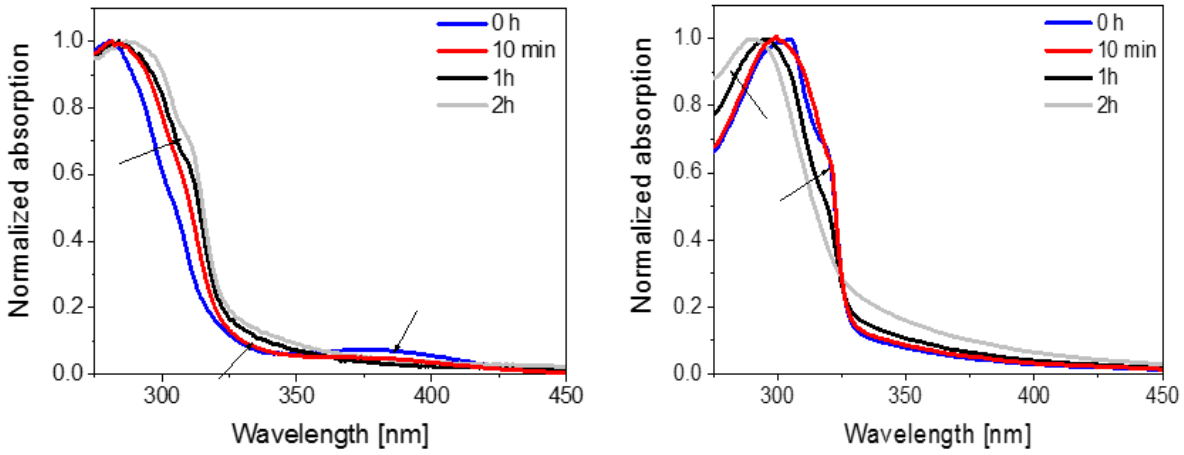


**Fig. 4.** Changes of the UV−vis absorption spectra of **1** (left) and **2** (right) measured in acetonitrile over time at 70 °C in dark.

This also holds with regard to the photostability studies. We monitored the changes of the absorption features under constant UV irradiation (302 nm) at room temperature (Figure 4). In stark contrast to the thermal stability study, the MLCT band of **1** disappears within the first minutes, while a Progressive red-shift of ~10 nm is noted for the absorption maxima of the LC band. This goes hand-in-hand with an overall broadening of this band due to the rising of a new shoulder located at ~320 nm. All-in-all, these results suggest the photoinduced formation of new species like $[Cu(POP)(MeCN)_2]^+$ and $[Cu(bpy)_2]^+$ (vide supra).[33,46,50,51] Interestingly, the absorption features of **2** hold constant during the first 10 min. For longer periods of time, the LC absorption band narrows, and the absorption maximum shows a blue-shift of ~15 nm. This suggests the partial unbonding of the diimine ligand forming the $[Cu(POP)(MeCN)(MeO\text{-}bpy)]^+$ complex.[51] Noteworthy, we discarded the formation of copper(II) species during the assays above, as the solutions did not turn greenish.

**Table 2.** Photoluminescence and Electrochemical Features of Complexes **1** and **2**.

| | Absorption | | Emission | | | | | Electrochemistry | |
|---|---|---|---|---|---|---|---|---|---|
| | $\lambda_{abs}$[a)] (nm) | $\lambda_{abs}$[b)] (nm) | $\lambda_{em}$[c)] (nm) | $\lambda_{em}$[d)] (nm) | $\Phi$[e)] | $\Phi$[f)] | $\tau$[g)] (μs) | $E_{ox}$[g)] (V) | $E_{red}$[g)] (V) |
| **1** | 289, 388 | 280, 380 | 585 | 590 | 0.06 | 0.09 | 0.83, 0.01 | +0.95 ($_{qr}$) | -2.00$_{(r)}$ -2.46$_{(r)}$ |
| **2** | 294, 415 | 306, 417 | 571 | 575 | 0.14 | 0.20 | 1.22, 0.13 | +1.00 ($_{qr}$) | -2.12$_{(r)}$ -2.51$_{(r)}$ |

[a]Measured at 298 K in dichloromethane. [b]Measured at 298 K in acetonitrile. [c]Photoluminescence spectra measured in powder at room temperature ($\lambda_{exc}$ 370 nm). [d]Photoluminescence spectra measured in thin film at room temperature ($\lambda_{exc}$ 370 nm). [e]Photoluminescence quantum yields measured in powder ($\lambda_{exc}$ 370 nm). [f]Photoluminescence quantum yields measured in thin film ($\lambda_{exc}$ 370 nm); excited-state lifetimes measured in powder ($\lambda_{exc}$ 370 nm). [g]Oxidation and reduction potentials measured versus $Cp_2Fe/Cp_2Fe^+$; qr = quasi reversible, r = reversible.

Concerning the photoluminescence features, both complexes are not emitting in both acetonitrile and dichloromethane solutions. However, they are strongly emissive in powder (Figure 5), showing a broad and featureless emission band centered at 580 and 570 nm for **1** and **2**, respectively. The emission shape indicates a similar charge-transfer (CT) nature for the emitting excited state, while the 10 nm blue-shifted emission of **2** compared to that of **1** is related to the difference of the dipole moment of the excited state.[44] The photoluminescence quantum yield (Φ) of **2** is much higher than that of **1**, that is, 0.14 versus 0.06 in the form of powder (Table 2), indicating a reduced nonradiative relaxation process in the excited state upon attaching methoxy groups. Importantly, thin films with the same composition as those used in devices also showed the same emission features associated with a similar trend for the Φ, that is, 0.20 versus 0.09 for **2** and **1**, respectively. This is in line with the longer excited-state lifetimes of **2** than those of 1 (Table 2). Overall, **2** features enhanced radiative and reduced nonradiative processes compared to those of **1**, suggesting that a better electroluminescence response with respect to luminance and efficacy might be expected in LECs.

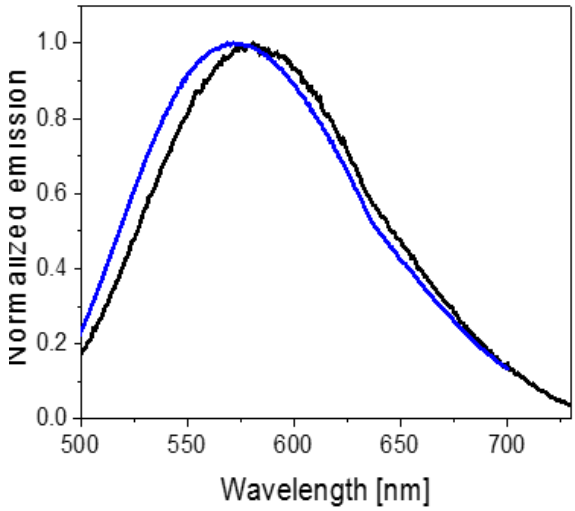


**Fig. 5.** Photoluminescence spectra of **1** (black) and **2** (blue) recorded at room temperature ($\lambda_{exc}$ 370 nm).

*2.3. Electrochemical Characterization.*

Cyclic voltammetry assays were performed for 1 and 2 in acetonitrile (see Experimental Section for further details). The cyclic voltammograms are displayed in Figure 6, while Table 2 summarized the oxidation and reduction potentials. In short, both the complexes showed the same quasi-reversible oxidation wave at ~1 V versus $Cp_2Fe/Cp_2Fe^+$. This is assigned to the typical metal-centered oxidation that forms copper(II) species.[47] In contrast, both complexes showed two reversible reduction waves located at −2.00/−2.46 V and −2.12/−2.51 V for **1** and **2**, respectively. This is attributed to the reduction of the bipyridyl ligand, and,[47] therefore, it is not surprising that the attachment of electrondonating groups shifts the reduction values toward higher potentials. In light of the electrochemical behavior, we can postulate that hole injection in both complexes could be critical for the device stability due to irreversible formation of oxidized species that can act as both emission quenchers and trap carriers.[52]

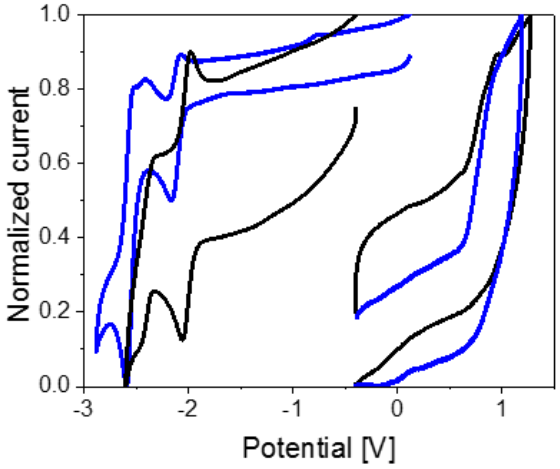


**Fig. 6.** Cyclic voltammograms of **1** (black line) and **2** (blue line) in acetonitrile.

*2.4. Electroluminescence Characterization: Effect of the Ligand Design.*

The electroluminescence features of **1** and **2** were studied at first in a standard single-layer LEC. Prior to the deposition of the active layer, a first layer of poly(3,4ethylenedioxythiophene):poly(styrenesulfonate) (PEDOT:PSS) (70 nm) was deposited onto patterned indium tin oxide (ITO) substrate to increase the device preparation yield. The active layer was prepared via spin-coating from fresh solutions of **1** or **2**. The thickness of the active layers was measured with α-step technique and was 120 nm. The devices were finalized depositing 90 nm of aluminum as cathode and were driven at various pulsed currents of 2.5, 5, and 7.5 mA, using a 1000 Hz block wave and a 50% duty cycle. Details concerning the device preparation and characterization are provided in the Experimental Section.

Regardless of the applied driving current, all the devices featured the same behavior over time (Figures 7 and 8). In detail, the average voltage profile showed a similar initial voltage peak at ~7 V followed by a slow decay up to a similar steadystate voltage regime at ~4−5 V (Figure 7). The average voltage refers to the half of the maximum voltage amplitude, as a 50% duty cycle is used. It is important to notice that the rise of the average voltage upon applying driving currents beyond 5 mA is quite likely related to over-oxidation processes that generate black spots.[53] Concerning the luminance, all the devices showed an instantaneous emission that increases up to its maximum within the first minutes under operation conditions (Figure 8). The electroluminescence (EL) spectra showed the same broad and unstructured band shape with maxima at 583 (**1**) and 573 (**2**) nm as observed in the photoluminescence measurements (Figure 9). This indicates that the same excited state is involved

regardless of the excitation mechanism. The x/y CIE color coordinates of 0.49/0.53 (**1**) and 0.46/0.52 (**2**) correspond to yellow-emitting devices.

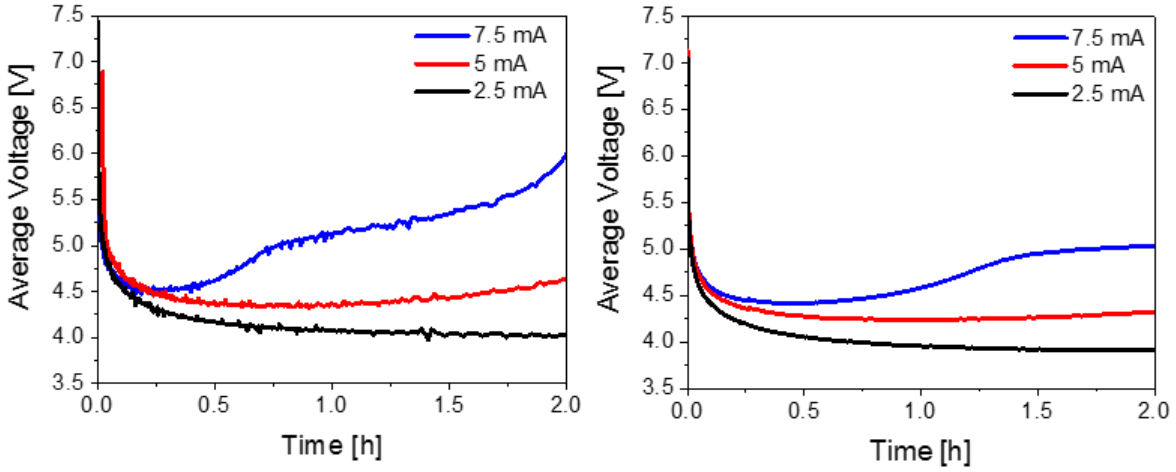


**Fig. 7.** Average voltage over time of devices with **1** (left) and **2** (right) driven at various pulsed currents.

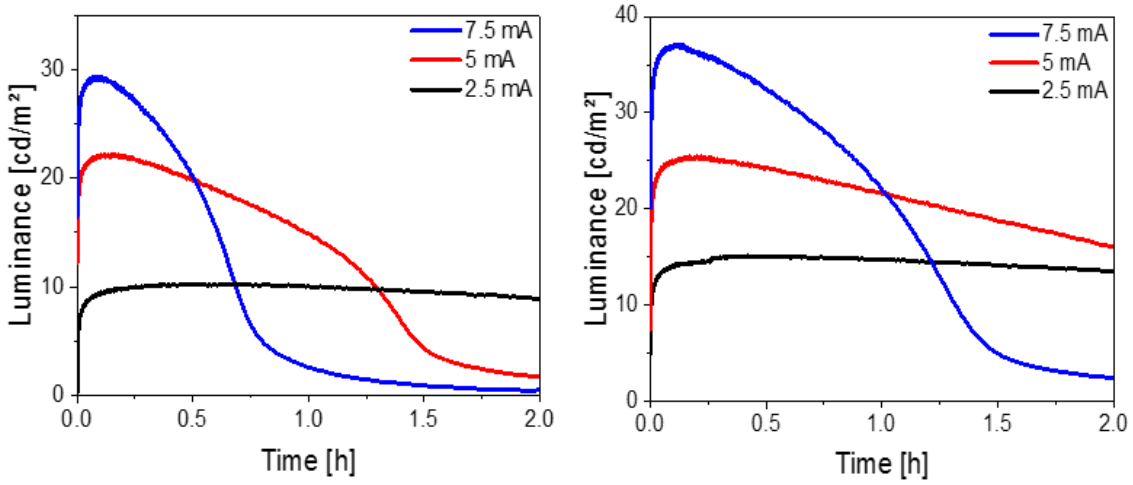


**Fig. 8.** Luminance over time of devices with **1** (left) and **2** (right) driven at various pulsed currents.

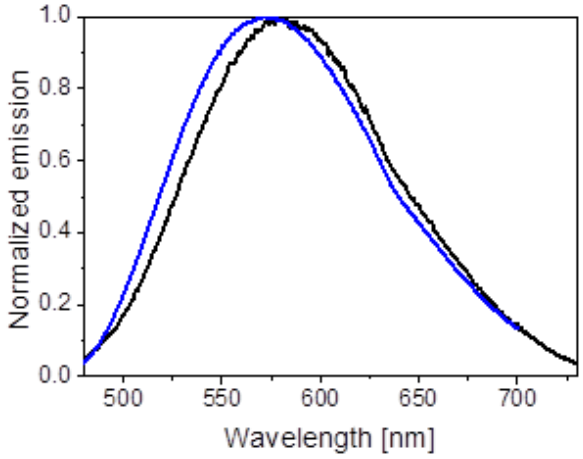


**Fig. 9.** Electroluminescence spectra of devices with **1** (black) and **2** (blue) driven at a pulsed current of 7.5 mA.

As summarized in Table 3, devices using **2** outperformed the reference devices with **1** in terms of luminance, efficiency, and lifetime. In particular, three- to fourfold higher efficiency was noted for

devices with **2**, reaching, for example, 0.4 cd/A at pulsed currents of 2.5 mA. As far as the stability is concerned, devices with **2** also presented a better stability with greater than fivefold longer lifetime using, for example, pulsed currents of 5 mA (Table 3). These results are in line with both the enhanced photoluminescence and stability features upon attaching the methoxy groups at the ortho position of diimine ligands (vide supra). On top of all of the aforementioned, it is also important to note that devices with 2 featured an overall low average voltage, while the turn-on time, that is, the time to reach the maximum luminance level, was significantly reduced compared to those with **1**. This suggested that the overall ionic mobility and, in turn, the EDLs formation was more efficient in devices with **2**.

**Table 3.** Figures of Merit of Devices Prepared with **1** and **2** Driven at Diff erent Pulsed Currents.

| | Driving current (mA) | Average Voltage (V) | $L_{inst}$[a)] ($cd/m^2$) | $L_{max}$[b)] ($cd/m^2$) | $t_{on}$[c)] (h) | $t_{1/2}$[d)] (h) | Efficacy (cd/A) | $\lambda_{em}$[e)] (x/y CIE coord.) |
|---|---|---|---|---|---|---|---|---|
| **1** | 2.5 | 4.0 | 0.3 | 10.2 | 0.90 | 5.5 | 0.1 | 587 (0.51/0.49) |
| **1** | 5.0 | 4.3 | 12.3 | 22.1 | 0.25 | 0.5 | 0.1 | |
| **1** | 7.5 | 4.5 | 16.6 | 28.5 | 0.20 | 0.6 | 0.1 | |
| **2** | 2.5 | 3.9 | 4.8 | 15.2 | 0.31 | 7.2 | 0.4 | 573 (0.46/0.52) |
| **2** | 5.0 | 4.2 | 7.8 | 25.1 | 0.12 | 2.6 | 0.3 | |
| **2** | 7.5 | 4.4 | 20.3 | 36.4 | 0.05 | 1.1 | 0.3 | |

[a]Instantaneous luminance or initial luminance level. [b]Maximum luminance. [c]Time to reach the maximum luminance. [d]Time to decay to the half of the maximum luminance. [e]Maximum in the electroluminescence spectrum of a fresh device (nm).

To further shed light onto this aspect, we performed electrochemical impedance spectroscopy (EIS) measurements at different applied voltages ranging from 0 to 5 V and frequencies going from 1 to $1 \cdot 10^6$ Hz.[20,54,55] EIS analyses of the Nyquist plots were conducted based on the equivalent circuit model provided in Figure S10. As shown in Figure S11, Nyquist plots consist of one semicircle whose diameter relates to the resistance associated with the dynamics of the EDLs formation at the electrode interface at applied voltages below the band gap of the emitters (<2.5 V) and the reduction of the intrinsic nondoped region, when charge injection is effective (>2.5 V). The changes of the resistance upon applying different voltages are displayed in Figure 10. At 0 V, devices with **1** show a significantly higher resistance value compared to those of **2**, that is, $1.51 \cdot 10^6$ versus $1.6 \cdot 10^5$ Ω. This resistance value is used to calculate the overall ionic mobility (σ) of the active layer (see Experimental Section for more information). In line with the turn-on time, devices with **2** featured a 10-fold higher σ ($5.3 \cdot 10^{-7}$ S/m) than that of devices with **1** ($5.1 \cdot 10^{-8}$ S/m). Furthermore, devices with **2** showed the typical exponential decay of the resistance related to the EDL formation until applied voltages close to 2.5 V (Figure 10).[20,54] This indicates that EDLs are easily formed due to the drifting of the mobile anions toward the electrode interfaces. In contrast, devices with **1** showed small changes in the resistance, until high voltages at ∼1.7 V are applied, while a similar injection voltage ($V_{inj}$) at ∼2.5 V was also noted.

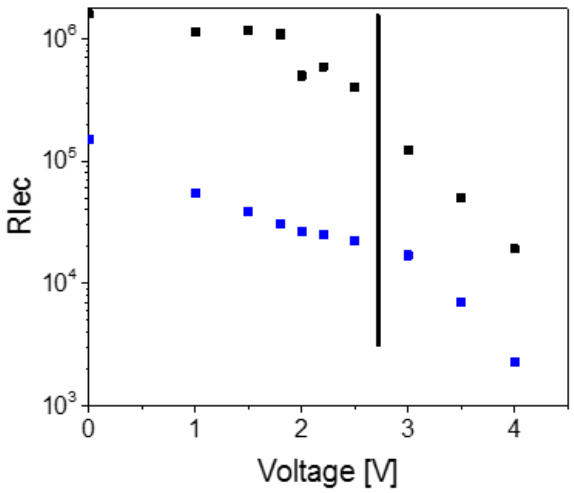


**Fig. 10.** Changes in Rlec of devices with **1** (black) and **2** (blue) under static EIS measurements. The injection voltage (Vinj ) is indicated with a solid black line.

Noteworthy, the resistance values of devices with **1** held 1 order of magnitude higher than those of devices with **2**. This finding could be related to either a different film morphology or a different cation−anion binding energy due to the sterical hindrance of the methoxy groups. The morphology of the active layers was therefore studied by using atomic force microscopy (AFM), Figure S12. Both layers show the same morphology with a less than 2% roughness and the absence of aggregates, holes, and/or a noticeable phase separation. This left the second hypothesis as the most plausible one that needs, however, a further corroboration.

*2.5. Electroluminescence Characterization: Effect of the Device Design.*

The new ligand design of complex **2** provides a significant enhancement with respect to the standard **1** in terms of efficacy and stability features due to the improved photoluminescence and ionic conductivity features in thin films. However, its moderate stability is still a concern. As noted by several authors, one of the major challenges in LECs involves the use of only one active compound for charge injection, transport, and emission processes.[2,3,6] This is critical in copper(I) complexes, as the oxidation process is irreversible (vide supra). Although the negative impact of forming irreversible oxidized species upon device operation conditions on the device stability has already been claimed, the underlying reasons have not been clarified yet.[41,52,56]

In an attempt to reduce the formation of the oxidized species, we proposed to decouple hole/electron injection and transport using a bilayer device architecture, in which a thin CBP (15 nm), that is, 4,4′-bis(9-carbazolyl)-1,1′-biphenyl, 4,4-N,N′-dicarbazole-1,1′-biphenyl)-layer separates the anode and active layer (Figure 11).

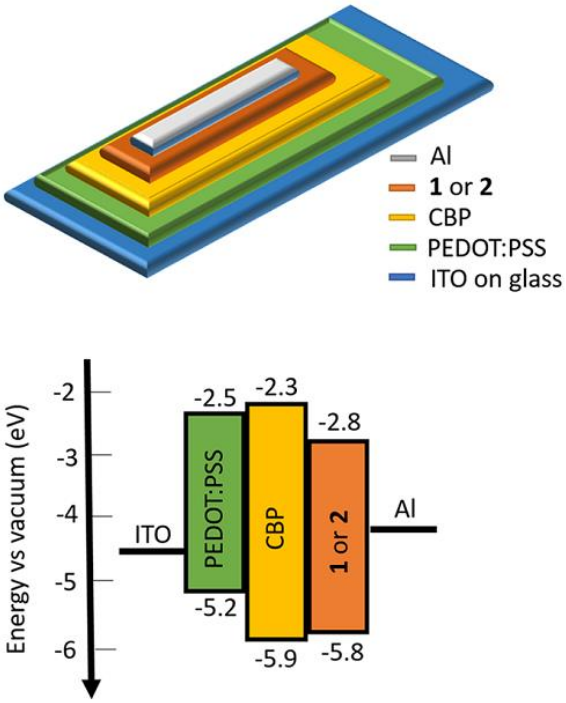


**Fig. 11.** Schemes of a bilayer device design (top) and its energy diagram (bottom) as derived from the CV data with the formula $E_{HOMO/LUMO} = e(V_{Cp/Cp^+}) + 4.8$ eV.

This compound was selected among other hole transport matrices due to (i) the reversible oxidation behavior at 1.1 V ensuring a stable p-electrochemical doping,[52] (ii) its wide electrochemical band gap, in which the highest-occupied molecular orbital (HOMO) and lowest-unoccupied molecular orbital (LUMO) levels of both 1 and 2 are embedded (Figure 11), ensuring an efficient electron-hole recombination at the CuiTMC layer, and (iii) its low solubility in acetonitrile, allowing the easy fabrication of devices by sequential spin-coating process from orthogonal solvents (see Experimental Section for further details).

We decided to drive these devices at 7.5 mA, which corresponds to the pulsed current that caused the least stability in the single-layer devices, along with a remarkable degradation in the active layer, as highlighted by the rise in the voltage after ∼0.5 and ∼1 h for 1 and 2, respectively (Table 3 and Figure 11). Similar to the single-layer devices, the LEC behavior was noted by the average voltage and luminance behaviors (Figure 12). While the luminance and efficacy remained very similar to those of the single-layer devices, for example, 32.9 cd/m$^2$ and 0.3 cd/ A versus 36.4 cd/m$^2$ and 0.3 cd/A for single and double LECs with **2**, respectively, the stability was significantly enhanced by **1** order of magnitude (Figures 12, 13, and S13, as well as Table 4). Noteworthy, devices with **2** always outperformed those with 1, regardless of the device architecture.

**Table 4.** Figures of Merit of Devices with CBP/1 and CBP/2 Architecture under a Pulsed Driving Current of 7.5 mA

| Device | Average voltage (V) | $L_{max}$ (cd/m$^2$) | $t_{on}$ (h) | $t_{1/2}$ (h) | Efficacy (cd/A) |
|---|---|---|---|---|---|
| CBP/**1** | 3.7 | 24.7 | 1.1 | 13 | 0.1 |
| CBP/**2** | 3.4 | 32.9 | 1.6 | 10.8 | 0.3 |

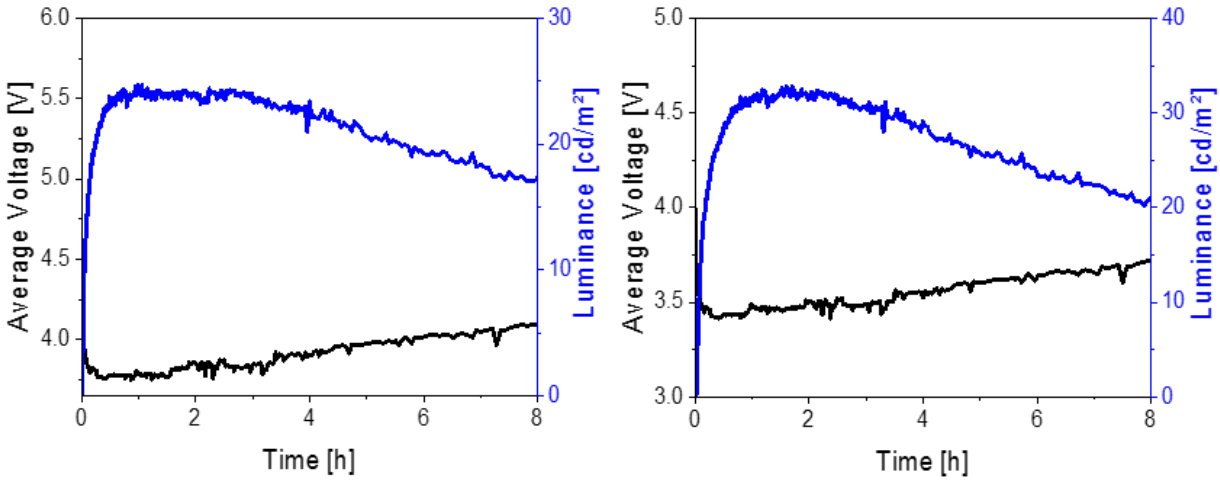


**Fig. 12.** Average voltage and luminance over time of devices with CBP/**1** (left) and CBP/**2** (right) driven at a pulsed current of 7.5 mA.

Since the EL spectra of the double-layer devices are similar to those of the single-layer devices without showing any EL feature of the CBP layer (Figures 13 and S13), we can postulate that electron−hole recombination efficiently occurs in the Cu-iTMC layers close at the interface CBP/Cu-iTMC. Since the hole energy barrier is the lowest one (Figure 11), hole injection occurs in the CBP layer, and then it is transferred to the CuiTMC, while electron injection and accumulation is effective in the Cu-iTMC emitting layer. As such, the formation of oxidized Cu-iTMC species is significantly reduced, leading to an enhanced device stability without affecting brightness and efficiency.

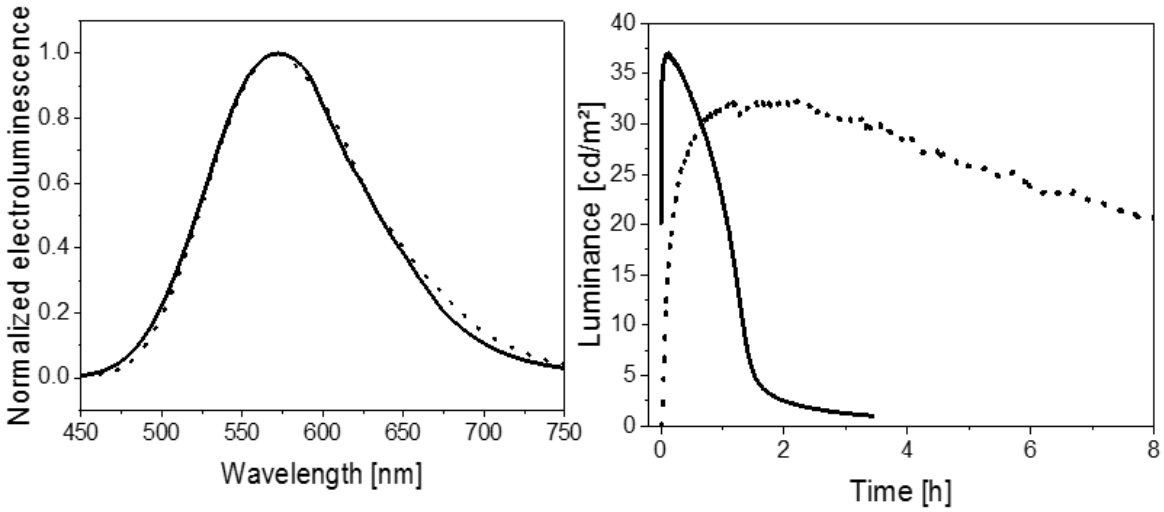


**Fig. 13.** EL spectra (left) and luminance (right) over time of the devices with **2** (solid line) and with CBP/**2** (dotted line) active layers driven at a pulsed current of 7.5 mA.

## 3 Conclusions

Two new findings on how to enhance the performance of LECs based on heteroleptic copper(I) complexes with the formula $[Cu(N^N)(P^P)]^+$ have been attained. First, we showed a new ligand design, obtained thanks to the symmetric insertion of two methoxy groups at the ortho position of the bpy ligand. The methoxy ligand combines high electron-donating properties, sterical hindrance, and a relatively high rotation freedom. This leads to superior photoluminescence and stability features, as demonstrated by spectroscopic and photo and thermal stability studies and XRD characterizations. These properties were also reflected in the EL features of single-layer LECs. Here, devices with the

new emitter showed a significant enhanced luminance, efficiency, and stability compared to those of reference devices with the archetypal copper(I) complex without any substituents. Second, further improvements were achieved introducing a new device design to decouple electron/hole injection and transport from electron−hole recombination. As evidenced by the electrochemical behavior of this family of copper(I) complexes, the formation of oxidized species is nonreversible. In addition, the effect of its accumulation under device operation conditions has not been fully understood yet. Herein, the double-layer architecture, in which a bottom CBP-based layer acts as hole injection/transport layer, and the top Cu-iTMC-based layer acts as an electron transport layer and emitting layer. Regardless of the applied Cu-iTMC, this device design leads to 10-fold enhanced stability without affecting the luminance and efficacy levels. As such, we can state that the search of novel device architectures might be key toward future breakthrough in the LECs based on the third generation of emitters.

## 4 Experimental section

### *4.1. Materials.*

All chemicals were purchased from chemical suppliers and used without further purification. All analytical reagentgrade solvents were purified by distillation. All reactions were performed under inert nitrogen atmosphere using standard vacuum lines techniques. PEDOT:PSS (Clevios PAl4083) was purchased from Heraeus. Microwave-assisted reactions were performed by a Biotage Initiator EXP synthesizer. Reactions were conducted in Biotage microwave vials, which were loaded using dried solvents. $^{1}H$, $^{13}C$, and $^{31}P$ NMR spectra were recorded on a JEOL ECP 400 spectrometer ($^{1}H$ NMR operating frequency 400 MHz) with chemical shifts referenced to residual protons of the solvent. The following abbreviations are used: s (singlet), d (doublet), t (triplet), dd (doublet of doublets), m (multiplet). Mass spectra were recorded on a Thermo-Finnigan Advantage Max Ion Trap Spectrometer equipped with an electrospray ion source (ESI).

### *4.2. Syntheses. 6,6′-Dimethoxy-2,2′-bipyridine.*

In a 20 mL Biotage microwave vial, $NiCl_2 \cdot 6\ H_2O$ (0.23 g, 1 mmol) and triphenylphosphine (4 mmol, 1.06 g) were put in 10 mL of dimethylformamide under $N_2$. Zinc powder (3 mmol, 0.19 g) was then added to the solution, which was stirred for 1 h at 50 °C. At this point, 2-bromo-6-methoxypyridine (1 mmol, 0.19 g) was added, and the solution was stirred for 20 h at 50 °C. The reaction mixture was then poured in 4 mL of 17% $NH_3$ and stirred for 1 h, and the aqueous phase was extracted three times with $CH_2Cl_2$. The reunited organic phases were dried with a rotavapor, and the residue was gathered in $CH_2Cl_2$. The product, a white solid, was then purified via flash column chromatography, to give yield to the desired 6,6′-dimethoxy-2,2′bipyridine (0.17 g, 0.8 mmol, 80%). $^{1}H$ NMR (400 MHz, $CDCl_3$): δ = 8.02 (d, J = 7.4 Hz, 2H), 7.68 (dd, J = 7.4, J = 8.2 Hz, 2H), 6.75 (d, J = 8.2 Hz, 2H), 4.04 (s, 6H) ppm. $^{13}C$ NMR (100 MHz, $CDCl_3$): δ = 163.5, 153.6, 139.4, 113.8, 111.0, 53.3 ppm. Mass m/z ($ESI^+$) for $C_{12}H_{12}N_2O_2$ calcd 216.09, found 216.07 $[M + H]^+$. Anal. Calcd (%) for $C_{12}H_{12}N_2O_2$: C 66.65, H 5.59, N 12.96, O 14.80; found: C 66.28, H 5.65, N 12.88, O 15.21.

### *[Cu(6,6′-dimethoxy-2,2′-bipyridine)(bis[2-(diphenylphosphino)phenyl]ether))]PF6 (**2**).*

In a 50 mL three-necked round-bottom flask $[Cu(CH_3CN)_4]PF_6$ (0.18 g, 0.5 mmol) and POP (0.29 g, 0.5 mmol) were mixed at room temperature under nitrogen. The solid reagents were then dissolved

in 15 mL of freshly distilled $CH_2Cl_2$, and the mixture was stirred at room temperature for 30 min. Then 15 mL of a degassed $CH_2Cl_2$ solution of 6,6′-dimethoxy-2,2′-bipyridine (0.11 g, 0.5 mmol) was added in the reaction flask, generating an instantaneous turn of the solution color from colorless to bright yellow. The solution was stirred for additional 30 min under $N_2$ at room temperature. The nitrogen flux was then removed, and the solvent was evaporated, providing a yellow solid powder. The solid was washed with diethyl ether to separate the product from the unreacted ligand. The purification was monitored via thin-layer chromatography (TLC) and afforded complex 2 (0.41 g, 87%). $^1$H NMR: (400 MHz, $CD_2Cl_2$): δ = 7.93 (t, J = 8.0 Hz, 2H), 7.74 (d, J = 7.6 Hz, 2H), 7.28−7.08 (m, 22H), 6.97 (t, J = 7.5 Hz, 2H), 6.86−6.81 (m, 4H), 6.72 (d, J = 8.3 Hz, 2H), 3.31 (s, 6H) ppm. $^{13}$C NMR (100 MHz, $CD_2Cl_2$): δ = 164.0, 158.6 (t, J = 6.1 Hz), 151.1, 141.9, 134.0, 133.5 (t, J = 8.0 Hz), 132.2 (t, J = 16.3 Hz), 131.7, 129.9, 128.6, 125.7 (t, J = 14.4 Hz), 124.7, 120.1, 115.3, 107.3, 55.1 ppm. $^{31}$P NMR (162 MHz, $CD_2Cl_2$): δ = −10.55 (broad s), −143.87 ($PF_6$ septet, J = 710.43 Hz) ppm. Mass m/z ($ESI^+$) for $C_{48}H_{40}N_2O_3P_2Cu$ calcd 817.18, found 816.20 $[M]^+$. Anal. Calcd (%) for $C_{48}H_{40}N_2O_3F_6P_3Cu$: C 59.85, H 4.19, N 2.91, O 4.98; found: C 59.99, H 4.38, N 2.83, O 5.32.

*4.3. X-ray Crystallography.*

Author: Please verify that the changes made to improve the English still retain your original meaning.
The crystal structures of **2** and of the ligand MeO-bpy alone were solved, and relevant crystallographic data are available in Table 1. Single-crystal diffraction data were collected using an Oxford Xcalibur CCD area detector diffractometer. Structure solution was performed by SIR2011,[57] and refinement with full-matrix least-squares was by SHELXL-2013.[58] Mercury was used for crystal structure drawing.[59] A suitable crystal was grown by slow evaporation of a 50:50 water/ acetone solution of **2**. Despite all crystallization attempts, the crystal grows in aggregates of very thin laminae. After it was checked optically and by a short XRD test a very small lamina was selected (Figure S2). The crystal, despite its reduced size and weakly diffracting nature, was suitable for structure solution and refinement, but it required a very long data collection (∼50 h with a single frame acquisition of 200 s). The internal agreement factor ($R_{int}$) and I/σ are good up to 2θ = 20 and reasonable up to 2θ = 30 (Figure S3). Beyond this limit, the number of unobserved reflections increase dramatically, similarly to $R_{int}$ values, but observed reflections are still present, and cutting these data would decrease the disagreement factors but also the data/parameter ratio. Therefore, all the collected data were used for the refinement, resulting more stable even if this choice generates some alerts in the checkcif. The distribution of distances and of anisotropic displacement parameter values confirms the stability of the refinement and the goodness of the data (Tables S1−S3). The structure that resulted was ordered similarly to that reported by Weber et al.[40] even for the $PF_6^-$ anion, which was often found disordered in similar structures.[60] Relevant XRD data are reported in Table 1, and geometric data are in Tables S1−S6 in the Supporting Information.
A transparent lamina was obtained by slow evaporation of MeO-bpy, dissolved in a 1:1 ethanol/water mixture. MeO-bpy crystallized unexpectedly in the non-centrosymmetric Pn21a space group. Attempt at solving MeO-bpy structure in Pnma space group resulted in a disordered structure with a not interpretable electron density. The good agreement of values and ADP parameters, together with the absence of serious alerts in the checkcif, confirm the space group assignation and the reliability of the structure. These peculiarities, along with some difficulties in its structure solution, might explain the current absence in the CCDC database, despite the molecule simplicity. Constraint of the ADP of corresponding atoms was employed, and a stable refinement was obtained, as indicated by

the good agreement values (Table S1) and by the reasonable obtained geometric (Tables S1 and S2) and atomic displacement parameters (ADP), Table S3. It is worth noting that MeO-bpy crystallizes in its neutral form as indicated by the absence of counteranions and by the packing consistent with a not-protonated nitrogen. In CCDC database most of the 6,6′-dimethoxy-2,2′bipyridine structures show a cationic form.[61] All the related crystal structures show the stable trans conformation like MeO-bpy, except that reported by Chan et al.,[62] where the NCCN torsion angle is equal to −129°. Concerning MeO-bpy packing, two subsets of parallel πstacking of the molecules and CH···O contacts of ∼2.5 Å, with each subset perpendicular to the adjacent subset.

*4.4. Theoretical Calculations.*

All the calculations were performed by the Gaussian 09 (G09) program package,[63] employing DFT method,[64] the Becke three-parameter hybrid functional,[65] the Lee− Yang−Parr[66] gradient-corrected correlation functional (B3LYP), and the 6-31G** basis set.[67]

4.5. Spectroscopic, Electrochemical, and Microscopy Characterization. The measurements under UV irradiation were performed with a UV lamp UVP 95-0199-01 model UVM-18 EL series hand-held UV lamp. Steady-state absorption spectra were recorded with a PerkinElmer Lambda 35. Steady-state emission spectra, photoluminescence quantum yields, and excited-state lifetimes were recorded with a fluoromax spectrometer from HORIBA Jobin Yvon IBH using an integrating sphere and the fluorescence and phosphorescence mode (measurement after 10 ns). AFM assays were performed with Veeco Dimension 5000 with a NanoScope V probe head and the Gwyddion evaluation software. Cyclic voltammetry was performed in acetonitrile solution, using the redox couple $Cp_2Fe$/ $Cp_2Fe^+$ as internal reference ($E_{1/2}$ = +0.40 V), a solution of tetrabuthylammonium hexafluorophosphate 0.1 M as electrolyte, and a glassy/carbon electrode as working electrode. The scan speed was 100 mV/s. It was measured with a Metrohm μAutolabIII potentiostat.

*4.6. Device Fabrication and Characterization.*

ITO substrates were purchased from Naranjo Substrates with ITO thickness of 130 nm. They were first cleaned with detergent, water, ethanol, and propan-2-ol as solvents in an ultrasonic bath (frequency 37−70 Hz, 30−40 °C) for 15 min each. Afterward, the slides were dried with $N_2$ gas and put in an UV-ozone cleaner for 8 min. A solution of PEDOT:PSS was filtered, sonicated, and mixed with propan-2-ol in a ratio of 3:1. The aforementioned solution (50 μL) was dropped onto the ITO, while the spin coater was rotating at a speed of 1500 rpm for 60 s giving rise to a thickness of 70 nm after drying the covered substrates for 10 min at 120 °C. The slides were then stored in a glovebox ($O_2$ level < 0.1 ppm, $H_2O$ level < 0.5 ppm). Complexes 1 and 2 were dissolved in acetonitrile with a concentration of 20 mg/mL. They were stirred in a closed vial for 10 min, and, if necessary, it was filtered. To obtain a thickness of ∼120 nm of active layer, the solution (75 μL) was spread onto the substrate that was later spin-coated with a speed of 1000 rpm for 50 s. The coated slides were then put in a glovebox and dried on a hot plate for 30 min at 90 °C. To obtain the biactive layer devices, a first layer of pristine CBP was deposited using a tetrahydrofuran (THF) solution of 2 mg/mL of the molecule and spin-coating it for 30 s at 3000 rpm; the parameters for 1 and 2 were the same as described before but with a concentration of 15 mg/mL. Once the active layer was deposited, the samples were transferred into an inert atmosphere glovebox (<0.1 ppm of $O_2$ and $H_2O$, Innovative Technology). Aluminum cathode electrode (90 nm) was thermally evaporated using a shadow mask under high vacuum (<$1 \times 10^{-6}$ mbar) using an Angstrom Covap evaporator integrated into the inert

atmosphere glovebox. The device statistics involve up to five different devices, that is, a total number of 20 pixels. Time dependence of luminance, voltage, and current was measured by applying constant and/or pulsed voltage and current by monitoring the desired parameters simultaneously by using Avantes spectrophotometer (Avaspec-ULS2048L-USB2) in conjunction with a calibrated integrated sphere Avasphere 30-Irrad and Botest OLT OLED LifetimeTest System. Electroluminescence spectra were recorded using the above-mentioned spectrophotometer. Electrochemical impedance spectroscopic assays were performed with a potentiostat/galvanostat (Metrohm μAutolabIII) equipped with a frequency response analyzer module (FRA2). Measurements were performed at the applied voltage range from 0 to 4 V and fitted with the Nova software using the circuit model shown in Figure S10. The alternating-current (AC) signal amplitude was set to 10 mV, modulated in a frequency range from 10 to 1 MHz. The Nova 1.11 software was used to obtain the parameters from the equivalent circuit. With these data at hand, the resistance of the intrinsic nondoped region ($R_i$) was directly obtained. The film conductivity (S/m) is measured at 0 V with the following equation: $\sigma = d/(AR_i)$, where d is the thickness of the layer, A is the area of the electrodes, and $R_i$ is the resistance of the active layer.

## Associated content

The Supporting Information is available free of charge on the ACS Publications website at DOI: 10.1021/acs.inorgchem.8b01914.
Characterization of MeO-bpy: chemical structure, $^{1}H$ and $^{13}C$ NMR, X-ray data, and theoretical study. Characterization of complex **2**: $^{1}H$, $^{13}C$, and $^{31}P$ NMR, X-ray, and absorption spectrum. Device characterization. EIS and AFM of the active layer. References. (PDF)
CCDC 1588140−1588141 contain the supplementary crystallographic data for this paper. These data can be obtained free of charge via www.ccdc.cam.ac.uk/data_request/cif, or by emailing data_request@ccdc.cam.ac.uk, or by contacting The Cambridge Crystallographic Data Centre, 12 Union Road, Cambridge CB2 1EZ, UK; fax: +44 1223 336033.

## Acknowledgments

E.F. and R.D.C. acknowledge the program “Ayudas para la atracción de talento investigador−Modalidad 1 of the Consejeria de Educació n, Juventud y Deporté −Comunidad de Madrid with the reference number 2016-T1/IND-1463”. R.D.C. acknowledges Spanish MINECO (RYC-2016-20891) for the Ramon y Cajal program (RYC-2016-20891).

## References

(1) Tang, S.; Edman, L.; Light-Emitting Electrochemical Cells: A Review on Recent Progress *Top Curr Chem* **2016**, *374*, 40.
(2) Fresta, E.; Costa, R. D.; Beyond Traditional Light-Emitting Electrochemical Cells – a Review of New Device Designs and Emitters *J. Mater. Chem. C* **2017**, *5*, 5643–5675.
(3) Costa, R. D.; *Light-Emitting Electrochemical Cells. Concepts, Advances and Challenges.* , 1st ed.; Costa, R. D., Ed.; Springer: Basel, 2017.
(4) Nardelli, A.; Deuschle, E.; de Azevedo, L. D.; Pessoa, J. L. N.; Ghisi, E.; Assessment of Light Emitting Diodes Technology for General Lighting: A Critical Review *Renew. Sustain. Energy Rev.* **2017**, *75*, 368–379.
(5) Housecroft, C. E.; Constable, E. C.; Over the LEC Rainbow: Colour and Stability Tuning of Cyclometallated Iridium(III) Complexes in Light-Emitting Electrochemical Cells *Coord. Chem. Rev.* **2017**, *350*, 155–177.

(6) Costa, R. D.; Ortí, E.; Bolink, H. J.; Monti, F.; Accorsi, G.; Armaroli, N.; Luminescent Ionic Transition-Metal Complexes for Light-Emitting Electrochemical Cells *Angew. Chemie - Int. Ed.* **2012**, *51*, 8178–8211.
(7) Matyba, P.; Yamaguchi, H.; Chhowalla, M.; Robinson, N. D.; Edman, L.; Flexible and Metal-Free Light-Emitting Electrochemical Cells Based on Graphene and PEDOT-PSS as the Electrode Materials *ACS Nano* **2011**, *5*, 574–580.
(8) Yu, Z.; Niu, X.; Liu, Z.; Pei, Q.; Intrinsically Stretchable Polymer Light-Emitting Devices Using Carbon Nanotube-Polymer Composite Electrodes *Adv. Mater.* **2011**, *23*, 3989–3994.
(9) Liang, J.; Li, L.; Niu, X.; Yu, Z.; Pei, Q.; Fully Solution-Based Fabrication of Flexible Light-Emitting Device at Ambient Conditions *J. Phys. Chem. C* **2013**, *117*, 16632–16639.
(10) Altal, F.; Gao, J.; Scanning Photocurrent and PL Imaging of a Frozen Polymer P-I-N Junction *Phys. Status Solidi - Rapid Res. Lett.* **2015**, *9*, 77–81.
(11) Matyba, P.; Maturova, K.; Kemerink, M.; Robinson, N. D.; Edman, L.; The Dynamic Organic P-N Junction. *Nat. Mater.* **2009**, *8*, 672–676.
(12) van Reenen, S.; Matyba, P.; Dzwilewski, A.; Janssen, R. A. J.; Edman, L.; Kemerink, M.; A Unifying Model for the Operation of Light-Emitting Electrochemical Cells *J. Am. Chem. Soc.* **2010**, *132*, 13776–13781.
(13) Sandstrom, A.; Dam, H. F.; Krebs, F. C.; Edman, L.; Ambient Fabrication of Flexible and Large-Area Organic Light-Emitting Devices Using Slot-Die Coating *Nat. Commun.* **2012**, *3*, 1002.
(14) Mauthner, G.; Landfester, K.; Köck, A.; Brückl, H.; Kast, M.; Stepper, C.; List, E. J. W.; Inkjet Printed Surface Cell Light-Emitting Devices from a Water-Based Polymer Dispersion *Org. Electron.* **2008**, *9*, 164–170.
(15) Sandstroem, A.; Asadpoordarvish, A.; Enevold, J.; Edman, L.; Spraying Light: Ambient-Air Fabrication of Large-Area Emissive Devices on Complex-Shaped Surfaces *Adv. Mater.* **2014**, *26*, 4975–4980.
(16) Weber, M. D.; Adam, M.; Tykwinski, R. R.; Costa, R. D.; Controlling the Chromaticity of Small-Molecule Light-Emitting Electrochemical Cells Based on TIPS-Pentacene *Adv. Funct. Mater.* **2015**, *25*, 5066–5074.
(17) Weber, K. T.; Karikis, K.; Weber, M. D.; Coto, P. B.; Charisiadis, A.; Charitaki, D.; Charalambidis, G.; Angaridis, P.; Coutsolelos, A. G.; Costa, R. D.; Cunning Metal Core: Efficiency/stability Dilemma in Metallated Porphyrin Based Light-Emitting Electrochemical Cells *Dalt. Trans.* **2016**, *45*, 13284–13288.
(18) Qian, G.; Lin, Y.; Wantz, G.; Davis, A. R.; Carter, K. R.; Watkins, J. J.; Saturated and Multi-Colored Electroluminescence from Quantum Dots Based Light Emitting Electrochemical Cells *Adv. Funct. Mater.* **2014**, *24*, 4484–4490.
(19) Aygüler, M. F.; Weber, M. D.; Puscher, B. M. D.; Medina, D. D.; Docampo, P.; Costa, R. D.; Light-Emitting Electrochemical Cells Based on Hybrid Lead Halide Perovskite Nanoparticles *J. Phys. Chem. C* **2015**, *119*, 12047–12054.
(20) Puscher, B. M. D.; Aygueler, M. F.; Docampo, P.; Costa, R. D.; Unveiling the Dynamic Processes in Hybrid Lead Bromide Perovskite Nanoparticle Thin Film Devices *Adv. Energy Mater.* **2017**, *7*, 1602283.
(21) Asadpoordarvish, A.; Sandström, A.; Larsen, C.; Bollström, R.; Toivakka, M.; Österbacka, R.; Edman, L.; Light-Emitting Paper *Adv. Funct. Mater.* **2015**, *25*, 3238–3245.
(22) Zhang, Z.; Li, Y.; Guan, G.; Li, H.; Luo, Y.; Zhao, F.; Zhang, Q.; Wei, B.; Pei, Q.; Peng, H.; et al.; A Colour-Tunable, Weavable Fibre-Shaped Polymer Light-Emitting Electrochemical Cell *Nat. Photonics* **2015**, *9*, 233–238.
(23) Lindh, E. M.; Sandström, A.; Andersson, M. R.; Edman, L.; Luminescent Line Art by Direct-Write Patterning *Light Sci. Appl.* **2016**, *5*, e16050.
(24) Weber, M. D.; Wittmann, J. E.; Burger, A.; Malcioglu, O. B.; Segarra-Martinez, J.; Hirsch, A.; Coto, P. B.; Bockstedte, M.; Costa, R. D.; From White to Red: Electric-Field Dependent Chromaticity of Light-Emitting Electrochemical Cells Based on Archetypal Porphyrins *Adv. Funct.*

*Mater.* **2016**, *26*, 6737–6750.
(25) Nishikitani, Y.; Takizawa, D.; Nishide, H.; Uchida, S.; Nishimura, S.; White Polymer Light-Emitting Electrochemical Cells Fabricated Using Energy Donor and Acceptor Fluorescent ??-Conjugated Polymers Based on Concepts of Band-Structure Engineering *J. Phys. Chem. C* **2015**, *119*, 28701–28710.
(26) Tang, S.; Pan, J.; Buchholz, H. a; Edman, L.; White Light from a Single-Emitter Light-Emitting Electrochemical Cell. *J. Am. Chem. Soc.* **2013**, *135*, 3647–3652.
(27) Henwood, A. F.; Zysman-Colman, E.; Luminescent Iridium Complexes Used in Light-Emitting Electrochemical Cells (LEECs) *Top. Curr. Chem.* **2016**, *374*, 36.
(28) Minaev, B.; Minaeva, V.; Ågren, H.; Theoretical Study of the Cyclometalated Iridium ( III ) Complexes Used as Chromophores for Organic Light-Emitting Diodes *J. Phys. Chem. A* **2009**, *113*, 726–735.
(29) Costa, R. D.; Monti, F.; Accorsi, G.; Barbieri, A.; Bolink, H. J.; Ortí, E.; Armaroli, N.; Photophysical Properties of Charged Cyclometalated Ir(III) Complexes: A Joint Theoretical and Experimental Study *Inorg. Chem.* **2011**, *50*, 7229–7238.
(30) Linfoot, C. L.; Leitl, M. J.; Richardson, P.; Rausch, A. F.; Chepelin, O.; White, F. J.; Yersin, H.; Robertson, N.; Thermally Activated Delayed Fluorescence (TADF) and Enhancing Photoluminescence Quantum Yields of $[Cu^{I}(Diimine)(diphosphine)]^{+}$ Complexes—Photophysical, Structural, and Computational Studies *Inorg. Chem.* **2014**, *53*, 10854–10861.
(31) Czerwieniec, R.; Leitl, M. J.; Homeier, H. H. H.; Yersin, H.; Cu(I) Complexes – Thermally Activated Delayed Fluorescence. Photophysical Approach and Material Design *Coord. Chem.Reviews* **2016**, *325*, 2–28.
(32) Onque, Y.; Hiraki, K.; Nishikawa, Y.; Interactions of Solid Supports and Fluorescent Substances in Thermally Activated Delayed Fluorescence. *Anal. Sci.* **1987**, *3*, 509–513.
(33) Armaroli, N.; Accorsi, G.; Cardinali, F.; Listorti, A.; Photochemistry and Photophysics of Coordination Compounds: Copper . In *Photochemistry and Photophysics of Coordination Compounds I*; Balzani, V., Campagna, S., Eds.; Springer Berlin Heidelberg, 2007; Vol. 280, pp 69–115.
(34) Lavie-Cambot, A.; Cantuel, M.; Leydet, Y.; Jonusauskas, G.; Bassani, D. M.; McClenaghan, N. D.; Improving the Photophysical Properties of Copper(I) Bis(phenanthroline) Complexes *Coord. Chem.Reviews* **2008**, *252*, 2572–2584.
(35) Bizzarri, C.; Strabler, C.; Prock, J.; Trettenbrein, B.; Ruggenthaler, M.; Yang, C. H.; Polo, F.; Iordache, A.; Brüggeller, P.; De Cola, L.; Luminescent Dinuclear Cu(I) Complexes Containing Rigid Tetraphosphine Ligands *Inorg. Chem.* **2014**, *53*, 10944–10951.
(36) Asil, D.; Foster, J. A.; Patra, A.; Dehatten, X.; Delbarrio, J.; Scherman, O. A.; Nitschke, J. R.; Friend, R. H.; Temperature- and Voltage-Induced Ligand Rearrangement of a Dynamic Electroluminescent Metallopolymer *Angew. Chemie Int. Ed.* **2014**, *53*, 8388–8391.
(37) Keller, S.; Constable, E. C.; Housecroft, C. E.; Neuburger, M.; Prescimone, A.; Longo, G.; Pertegás, A.; Sessolo, M.; Bolink, H. J.; [Cu(bpy)(P^P)] + Containing Light-Emitting Electrochemical Cells: Improving Performance through Simple Substitution *Dalt. Trans.* **2014**, *43*, 16593–16596.
(38) Keller, S.; Pertegás, A.; Longo, G.; Martínez, L.; Cerdá, J.; Junquera-Hernández, J. M.; Prescimone, A.; Constable, E. C.; Housecroft, C. E.; Ortí, E.; et al.; Correction: Shine Bright or Live Long: Substituent Effects in $[Cu(N^N)(P^P)]^{+}$ -Based Light-Emitting Electrochemical Cells Where N^N Is a 6-Substituted 2,2′-Bipyridine *J. Mater. Chem. C* **2016**, *4*, 3872–3872.
(39) Brunner, F.; Martínez-Sarti, L.; Keller, S.; Pertegás, A.; Prescimone, A.; Constable, E. C.; Bolink, H. J.; Housecroft, C. E.; Peripheral Halo-Functionalization in [Cu(N^N)(P^P)](+) Emitters: Influence on the Performances of Light-Emitting Electrochemical Cells. *Dalt. Trans.* **2016**, *45*, 15180–15192.
(40) Weber, M. D.; Garino, C.; Volpi, G.; Casamassa, E.; Milanesio, M.; Barolo, C.; Costa, R. D.; Origin of a Counterintuitive Yellow Light-Emitting Electrochemical Cell Based on a Blue-Emitting

Heteroleptic Copper(I) Complex *Dalt. Trans.* **2016**, *45*, 8984–8993.
(41) Elie, M.; Sguerra, F.; Di Meo, F.; Weber, M. D.; Marion, R.; Grimault, A.; Lohier, J. F.; Stallivieri, A.; Brosseau, A.; Pansu, R. B.; et al.; Designing NHC-Copper(I) Dipyridylamine Complexes for Blue Light-Emitting Electrochemical Cells *ACS Appl. Mater. Interfaces* **2016**, *8*, 14678–14691.
(42) Mohankumar, M.; Monti, F.; Holler, M.; Niess, F.; Delavaux-Nicot, B.; Armaroli, N.; Sauvage, J. P.; Nierengarten, J. F.; Combining Topological and Steric Constraints for the Preparation of Heteroleptic Copper(I) Complexes *Chem. - A Eur. J.* **2014**, *20*, 12083–12090.
(43) Kaeser, A.; Mohankumar, M.; Mohanraj, J.; Monti, F.; Holler, M.; Cid, J.-J.; Moudam, O.; Nierengarten, I.; Karmazin-Brelot, L.; Duhayon, C.; et al.; Heteroleptic Copper(I) Complexes Prepared from Phenanthroline and Bis-Phosphine Ligands *Inorg. Chem.* **2013**, *52*, 12140–12151.
(44) Weber, M. D.; Viciano-Chumillas, M.; Armentano, D.; Cano, J.; Costa, R. D.; σ-Hammett Parameter: A Strategy to Enhance Both Photo- and Electro-Luminescence Features of Heteroleptic Copper(I) Complexes *Dalt. Trans.* **2017**, *46*, 6312–6323.
(45) Costa, R. D.; Tordera, D.; Ortí, E.; Bolink, H. J.; Schönle, J.; Graber, S.; Housecroft, C. E.; Constable, E. C.; Zampese, J. A.; Copper(i) Complexes for Sustainable Light-Emitting Electrochemical Cells *J. Mater. Chem.* **2011**, *21*, 16108–16118.
(46) Kuang, S.-M.; Cuttell, D. G.; McMillin, D. R.; Fanwick, P. E.; Walton, R. A.; Synthesis and Structural Characterization of Cu(I) and Ni(II) Complexes That Contain the Bis[2-(Diphenylphosphino)phenyl]ether Ligand. Novel Emission Properties for the Cu(I) Species *Inorg. Chem.* **2002**, *41*, 3313–3322.
(47) Andrés-Tomé, I.; Fyson, J.; Baiao Dias, F.; Monkman, A. P.; Iacobellis, G.; Coppo, P.; Copper(I) Complexes with Bipyridyl and Phosphine Ligands: A Systematic Study *Dalt. Trans.* **2012**, *41*, 8669–8674.
(48) Nelson, T. D.; Crouch, R. D.; Cu, Ni, and Pd Mediated Homocoupling Reactions in Biaryl Syntheses: The Ullmann Reaction. *Org. React.* **2004**, *63*, 265–555.
(49) Kaeser, A.; Moudam, O.; Accorsi, G.; Séguy, I.; Navarro, J.; Belbakra, A.; Duhayon, C.; Armaroli, N.; Delavaux-Nicot, B.; Nierengarten, J. F.; Homoleptic Copper(I), Silver(I), and Gold(I) Bisphosphine Complexes *Eur. J. Inorg. Chem.* **2014**, *2014*, 1345–1355.
(50) Yuasa, J.; Dan, M.; Kawai, T.; Phosphorescent Properties of Metal-Free Diphosphine Ligands and Effects of Copper Binding *Dalt. Trans.* **2013**, *42*, 16096–16101.
(51) Armaroli, N.; Photoactive Mono- and Polynuclear Cu(I)–phenanthrolines. A Viable Alternative to Ru(II)–polypyridines? *Chem. Soc. Rev.* **2001**, *30*, 113–124.
(52) Lundberg, P.; Lindh, E. M.; Tang, S.; Edman, L.; Towards Efficient and Metal-Free Emissive Devices: A Solution-Processed Host-Guest Light-Emitting Electrochemical Cell Featuring Thermally Activated Delayed Fluorescence *ACS Appl. Mater. Interfaces* **2017**, *9*, 28810–28816.
(53) Gao, Y.; MacKenzie, R. C. I.; Liu, Y.; Xu, B.; Van Loosdrecht, P. H. M.; Tian, W.; Engineering Ultra Long Charge Carrier Lifetimes in Organic Electronic Devices at Room Temperature *Adv. Mater. Interfaces* **2015**, *2*, 1400555.
(54) Munar, A.; Sandström, A.; Tang, S.; Edman, L.; Shedding Light on the Operation of Polymer Light-Emitting Electrochemical Cells Using Impedance Spectroscopy *Adv. Funct. Mater.* **2012**, *22*, 1511–1517.
(55) Van Reenen, S.; Janssen, R. A. J.; Kemerink, M.; Dynamic Processes in Sandwich Polymer Light-Emitting Electrochemical Cells *Adv. Funct. Mater.* **2012**, *22*, 4547–4556.
(56) Wågberg, T.; Hania, P. R.; Robinson, N. D.; Shin, J. H.; Matyba, P.; Edman, L.; On the Limited Operational Lifetime of Light-Emitting Electrochemical Cells *Adv. Mater.* **2008**, *20*, 1744–1749.
(57) Burla, M. C.; Caliandro, R.; Camalli, M.; Carrozzini, B.; Cascarano, G. L.; Giacovazzo, C.; Mallamo, M.; Mazzone, A.; Polidori, G.; Spagna, R.; SIR2011: A New Package for Crystal Structure Determination and Refinement *J. Appl. Crystallogr.* **2012**, *45*, 357–361.
(58) Sheldrick, G. M.; Experimental Phasing with SHELXC/D/E: Combining Chain Tracing with

Density Modification *Acta Crystallogr. Sect. D Biol. Crystallogr.* **2010**, *66*, 479–485.
(59) Macrae, C. F.; Bruno, I. J.; Chisholm, J. A.; Edgington, P. R.; McCabe, P.; Pidcock, E.; Rodriguez-Monge, L.; Taylor, R.; Van De Streek, J.; Wood, P. A.; Mercury CSD 2.0 - New Features for the Visualization and Investigation of Crystal Structures *J. Appl. Crystallogr.* **2008**, *41*, 466–470.
(60) Gobetto, R.; Nervi, C.; Romanin, B.; Salassa, L.; Milanesio, M.; Croce, G.; X-Ray Structures and Complete NMR Assignment by DFT Calculations of [Os(bpy)2(CO)Cl]PF6 and [Os(bpy)2(CO)H]PF6 Complexes *Organometallics* **2003**, *22*, 4012–4019.
(61) Bator, G.; Sawka-Dobrowolska, W.; Sobczyk, L.; Grech, E.; Nowicka-Scheibe, J.; Pawlukojć, A.; Wuttke, J.; Baran, J.; Owczarek, M.; 4,4′-, 5,5′-, and 6,6′- Dimethyl-2,2′-Bipyridyls: The Structures, Phase Transitions, Vibrations, and Methyl Group Tunneling of Their Complexes with Chloranilic Acid *J. Chem. Phys.* **2011**, *135*, 44509.
(62) Chan, B. C. K.; Baird, M. C.; Reactions of 6,6′-Dimethyl-2,2′-Bipyridyl with Iron(II) in Aqueous and Non-Aqueous Media *Inorganica Chim. Acta* **2004**, *357*, 2776–2782.
(63) Frisch, M. J.; Trucks, G. W.; Schlegel, H. B.; Scuseria, G. E.; Robb, M. A.; Cheeseman, J. R.; G. Scalmani, V.; Barone, B.; Mennucci, G. A.; Petersson, H.; et al.; Gaussian09 *Gaussian,Inc., Wallingford CT,Gaussian 09,Revis.E.01* **2009**.
(64) Casida, M. E.; Jamorski, C.; Casida, K. C.; Salahub, D. R.; Molecular Excitation Energies to High-Lying Bound States from Time-Dependent Density-Functional Response Theory: Characterization and Correction of the Time-Dependent Local Density Approximation Ionization Threshold *J. Chem. Phys.* **1998**, *108*, 4439–4449.
(65) Becke, A. D.; Density-functional Thermochemistry. III. The Role of Exact Exchange *J. Chem. Phys.* **1993**, *98*, 5648–5652.
(66) Lee, C.; Yang, W.; Parr, R. G.; Development of the Colle-Salvetti Correlation-Energy Formula into a Functional of the Electron Density *Phys. Rev. B* **1988**, *37*, 785–789.
(67) McLean, A. D.; Chandler, G. S.; Contracted Gaussian Basis Sets for Molecular Calculations. I. Second Row Atoms, *Z* =11–18 *J. Chem. Phys.* **1980**, *72*, 5639–5648.